Entry, Flux, and Exit of Potential Vorticity in Ocean Circulation

JOHN MARSHALL, DANIEL JAMOUS, AND JOHAN NILSSON*

Program in Atmospheres, Oceans, and Climate, Department of Earth, Atmospheric, and Planetary Sciences, Massachusetts Institute of Technology, Cambridge, Massachusetts

(Manuscript received 21 July 1998, in final form 31 May 2000)

ABSTRACT

The flux form of the potential vorticity (PV) equation is employed to derive simple expressions for the boundary and interior flux of PV in ocean circulation using Bernoulli functions. The formulas are discussed and physically interpreted and used to map the flux of PV through a model of ocean circulation.

1. Introduction

The entry and exit of potential vorticity into ocean circulation, and the flux of potential vorticity through it, can be elegantly and succinctly described in the framework provided by the flux form of the potential vorticity equation (see Marshall and Nurser 1992, hereafter MN):

$$\frac{\partial}{\partial t}(\rho Q) + \nabla \cdot \mathbf{J} = 0, \tag{1}$$

where $\mathbf{J}$ is a generalized flux of potential vorticity Q,

$$Q = -\frac{1}{\rho}\boldsymbol{\omega} \cdot \nabla\sigma \tag{2}$$

with

$$\boldsymbol{\omega} = 2\boldsymbol{\Omega} + \nabla \times \mathbf{u} \tag{3}$$

the absolute vorticity, ρ the density, and σ the potential density.

The conservation law, Eq. (1), which will be discussed further in section 2, has a number of notable properties:

- No matter what thermodynamic variable is chosen to define the potential vorticity (PV) and what equation of state is assumed, the mass-weighted PV can *always* be written as the divergence of a vector and hence a flux-form PV equation can always be written for an appropriately defined $\mathbf{J}$ (see section 2);
- the rhs of Eq. (1) is *identically* zero, even in the presence of sources of momentum and buoyancy;
- there is a constraint on the $\mathbf{J}$ vectors: the flux $\mathbf{J}$ cannot pass through a σ surface—σ surfaces are *impermeable* to potential vorticity (see Haynes and McIntyre 1987; MN).

In this paper we discuss and illustrate the interesting perspective on ocean circulation provided by (1) and its attendant theorems. In particular, we focus on the quantification of the entry of potential vorticity through surface outcrops and its interior path through the ocean back to the surface or solid boundaries. The results of MN are generalized to include thermobaric effects exploiting the Bernoulli framework introduced by Schär (1993) and Bretherton and Schär (1993). We derive integral relationships that express the net flux of PV through the sea surface within closed Bernoulli contours or integrated between σ surfaces across the ocean from one coast to the other.

In section 2 we present the relevant theory setting out the diagnostic framework. In section 3 we illustrate the ideas by diagnosis of the PV fluxes in a numerical model of the North Atlantic. In section 4 we discuss the perspective on ocean circulation provided by the flux form of the potential vorticity equation.

2. Background theory

a. The PV flux and the flux form of the PV equation

The flux form of the PV equation has been explored in Haynes and McIntyre (1987), MN, Rhines (1993), Schär (1993), and Bretherton and Schär (1993). It was first discussed in the context of ocean circulation by MN, but in that theoretical development no account was taken of thermobaric effects nor was use made of the

* Current affiliation: Department of Meteorology, University of Stockholm, Stockholm, Sweden.

Corresponding author address: Dr. John Marshall, Dept. of Earth, Atmospheric, and Planetary Sciences, Massachusetts Institute of Technology, Room 54-1526, Cambridge, MA 02139-4307.
E-mail: marshall@gulf.mit.edu

Bernoulli framework introduced by Schär (1993) and Bretherton and Schär (1993). Here we consider an ocean with an arbitrary equation of state (but retain the Boussinesq approximation) and take on board the developments introduced by Schär (1993) and Bretherton and Schär (1993). The salient issues and concepts that attend the flux form of the PV equation are rather subtle, so here we highlight key steps in the derivation of diagnostic relations for a stratified ocean based on it. To further clarify issues we have also included, in an appendix, a parallel discussion for the simpler and more familiar problem of Stommel's ocean gyre (Stommel 1948). There, in a homogeneous ocean, **J** vectors begin and end on solid boundaries, but in a stratified ocean, **J** vectors can thread down from the sea surface through outcrop windows.

Following Bretherton and Schär (1993) we can write, making use of the definition of PV, (2), and noting that $\nabla \cdot \boldsymbol{\omega} = 0$:

$$\frac{\partial}{\partial t}(\rho Q) = \frac{\partial}{\partial t}(-\boldsymbol{\omega} \cdot \nabla\sigma) = -\frac{\partial}{\partial t}\nabla \cdot (\boldsymbol{\omega}\sigma) = -\nabla \cdot \mathbf{j}, \quad (4)$$

where the vector **j** is[1]

$$\mathbf{j} = \frac{\partial}{\partial t}(\boldsymbol{\omega}\sigma).$$

As noted by Haynes and McIntyre (1987), and Bretherton and Schär (1993), the above is true for any scalar field σ and nondivergent vector $\boldsymbol{\omega}$. A mathematical identity, (4) shows that one can always write a conservation law for PV in flux form, because ρQ can always be written as the divergence of a vector. Thus, as yet, Eq. (4) is devoid of any physical meaning. Moreover, if one adds any nondivergent vector to **j,** Eq. (4) will always be satisfied. For **j** to have any physical meaning we must choose an appropriate ''gauge.''

Expanding the partial derivative in **j**, one can write

$$\mathbf{j} = \boldsymbol{\omega}\frac{\partial\sigma}{\partial t} + \sigma\frac{\partial\boldsymbol{\omega}}{\partial t}.$$

Now, using (3) and the vector identity $\nabla \times (a\mathbf{A}) = a\nabla \times \mathbf{A} + \nabla a \times \mathbf{A}$, where a is a scalar and **A** a vector, one can write

$$\mathbf{j} = \boldsymbol{\omega}\frac{\partial\sigma}{\partial t} + \frac{\partial\mathbf{u}}{\partial t} \times \nabla\sigma + \nabla \times \left(\sigma\frac{\partial\mathbf{u}}{\partial t}\right).$$

The third term is nondivergent and hence does not contribute to (4). Our problem, now, is to determine a nondivergent gauge **X** such that the flux **J,**

$$\mathbf{J} = \boldsymbol{\omega}\frac{\partial\sigma}{\partial t} + \frac{\partial\mathbf{u}}{\partial t} \times \nabla\sigma + \mathbf{X}, \quad (5)$$

has physical significance.[2] The gauge **X** is chosen so that (5) is consistent with an alternative expression for **J** obtained (as a prelude to forming the potential vorticity equation) by crossing the momentum equation by $\nabla\sigma$ as follows.

The Boussinesq momentum equation is given by

$$\frac{\partial\mathbf{u}}{\partial t} = -\boldsymbol{\omega} \times \mathbf{u} - \nabla\left(\frac{|\mathbf{u}|^2}{2} + \frac{p}{\rho_o}\right) - \frac{\rho'}{\rho_o}\nabla\Phi + \mathbf{F}, \quad (6)$$

where p is the deviation of the pressure from that of a resting, hydrostatically balanced ocean, Φ is the geopotential, and **F** is the (nonconservative) frictional force per unit mass. Following Schär (1993) we write

$$\frac{\rho'}{\rho_o}\nabla\Phi = \nabla\left(\frac{\rho'}{\rho_o}\Phi\right) - \frac{\Phi}{\rho_o}\nabla\rho'$$

and take the cross product of Eq. (6) with $\nabla\sigma$ to obtain

$$\frac{\partial\mathbf{u}}{\partial t} \times \nabla\sigma = -(\boldsymbol{\omega} \times \mathbf{u}) \times \nabla\sigma - \nabla\pi \times \nabla\sigma + \frac{\Phi}{\rho_o}\nabla\rho' \times \nabla\sigma + \mathbf{F} \times \nabla\sigma, \quad (7)$$

where

$$\pi = M + \frac{|\mathbf{u}|^2}{2} \quad (8)$$

is a Bernoulli function and

$$M = \frac{p}{\rho_o} + \frac{\rho'}{\rho_o}\Phi \quad (9)$$

is the Montgomery potential.

Noting that $\nabla\sigma \times (\boldsymbol{\omega} \times \mathbf{u}) = \boldsymbol{\omega}(\nabla\sigma \cdot \mathbf{u}) - \mathbf{u}(\nabla\sigma \cdot \boldsymbol{\omega})$, Eq. (7) may be rearranged and written thus:

$$\mathbf{J} = \boldsymbol{\omega}\frac{\partial\sigma}{\partial t} + \left(\frac{\partial\mathbf{u}}{\partial t} + \nabla\pi\right) \times \nabla\sigma, \quad (10)$$

where

$$\mathbf{J} = \rho Q\mathbf{u} + \boldsymbol{\omega}\frac{D\sigma}{Dt} + \mathbf{F} \times \nabla\sigma + \frac{\Phi}{\rho_o}\nabla\rho' \times \nabla\sigma \quad (11)$$

is the PV flux written down in MN [Eqs. (1b) and (1c)], but modified by the nonadvective term $\rho_o^{-1}\Phi\nabla\rho' \times \nabla\sigma$ due to variations in in situ density along σ surfaces caused by thermobaric effects. The latter term is zero if $\sigma = \sigma(\rho')$—for example, if, as in MN, we ignore the pressure dependence of ρ'. However, in the general case $\nabla\rho' \times \nabla\sigma \neq 0$. Note that now Lagrangian conservation of PV no longer pertains even in adiabatic, frictionless flow—see McDougall (1988)—but a flux form of the PV equation can always be written.

[1] A lower case **j** is used here because the ''gauge'' has not yet been determined.

[2] $\mathbf{X} = 0$ is not a satisfying choice because it would imply, as noted by Bretherton and Schär (1993), that $\mathbf{J} = 0$ in the steady state.

Equation (10) is the same as (5), provided we choose the gauge to be

$$\mathbf{X} = \nabla\pi \times \nabla\sigma. \tag{12}$$

Equations (10) and (11) are alternative and equivalent definitions of the **J** vector—on equating them we obtain (7), a component of the momentum equation. MN's discussion was based on (11). But (10) also has great utility, and is the central focus of the present study, because it

1) reveals the ''impermeability theorem'' in a transparent way—the first term on the lhs, when projected in the direction normal to the σ surface, is equal to $v_\sigma \rho Q$, where $v_\sigma = -|\nabla\sigma|^{-1}\partial\sigma/\partial t$ is the velocity of the σ surface normal to itself. The remaining terms represent a flux that is always parallel to the σ surface.
2) shows that **J** can be diagnosed without explicit reference to frictional (**F**) and buoyancy ($D\sigma/Dt$) sources, if $\partial\sigma/\partial t$ and $\partial\mathbf{u}/\partial t$ are known.
3) shows that in the steady state π is the streamfunction for the **J** vector on σ surfaces, even in the presence of frictional and buoyancy sources, a very general result first noted by Schär (1993) and Bretherton and Schär (1993) and labeled as the ''generalized Bernoulli theorem.''

b. The PV flux through the sea surface

A quantification of the entry of PV into ocean circulation through the surface outcrops is of great interest because it must match the advective flux away from the sea surface in the stratified interior. Here, we rederive a result of MN [their Eq. (16)] but start from Eq. (10) rather than, as in MN, (11). From (10), we write the upward PV flux at the sea surface J_z as

$$J_z = \omega_z \frac{\partial\sigma}{\partial t} + \mathbf{k}\cdot\left(\frac{\partial\mathbf{u}}{\partial t} + \nabla\pi\right) \times \nabla\sigma, \tag{13}$$

where $\mathbf{k}$ and ω_z are, respectively, the unit vector and the component of the absolute vorticity in the vertical direction. By using the vector identity $\mathbf{A}\cdot(\mathbf{B}\times\mathbf{C}) = (\mathbf{A}\times\mathbf{B})\cdot\mathbf{C}$ and noting that $\mathbf{k}\times\nabla\Phi = 0$, we have

$$J_z = \omega_z \frac{\partial\sigma}{\partial t} + \mathbf{k}\times\left[\frac{\partial\mathbf{u}}{\partial t} + \nabla\left(\frac{|\mathbf{u}|^2}{2} + \frac{p}{\rho_o}\right)\right]\cdot\nabla\sigma. \tag{14}$$

Clearly to lowest order in the Rossby number, Eq. (14) yields the formula [Eq. (16)] of MN:

$$J_z = f\left(\frac{\partial\sigma}{\partial t} + \mathbf{u}_g\cdot\nabla\sigma\right), \tag{15}$$

where f is the Coriolis parameter and

$$\mathbf{u}_g = \frac{1}{\rho_o f}\mathbf{k}\times\nabla p$$

is the geostrophic velocity. Marshall and Nurser arrived at (15) starting from (11), but the derivation here, beginning from (10), is much more direct and general and clearly shows that J_z can be diagnosed without direct reference to buoyancy or mechanical forcing.

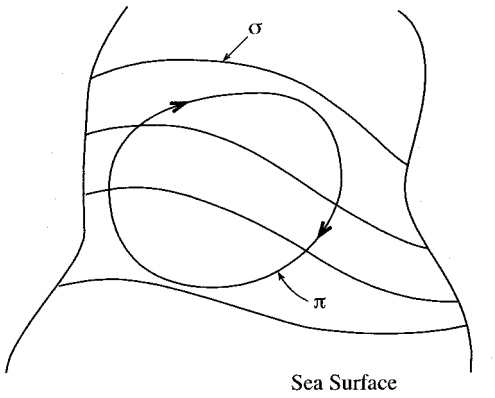

FIG. 1. Schematic diagram showing contours of Bernoulli function π and potential density σ at the sea surface. Typically, outcrops (contours defined by σ cutting the sea surface) do not close on themselves, but π surfaces often do.

In the steady state—we consider time dependence in section 2d—Eq. (13) can be written

$$J_z = \nabla\cdot[\mathbf{k}\times(\nabla\pi)\sigma] = \frac{\partial(\pi,\sigma)}{\partial(x,y)}, \tag{16}$$

where $\partial(\pi,\sigma)/\partial(x,y)$ is the Jacobian of π and σ evaluated at the sea surface. In the steady state Eq. (16) tells us that

- J_z vanishes locally whenever π and σ are aligned
- by Gauss theorem, the integral of J_z vanishes over a region of the sea surface bounded by contours of constant π or σ. Typically, as sketched in Fig. 1, outcrops (contours defined by σ cutting the sea surface) do not close on themselves, but π surfaces often do.
- $J_z > 0$ (i.e., the PV flux is directed *out* of the ocean) in regions where $\mathbf{u}_g\cdot\nabla\sigma > 0$ (and vice versa)—in the Northern Hemisphere—we sketch the state of affairs in Fig. 1.

1) INTEGRAL STATEMENTS

Let us define $\hat{J}_z$ as the total PV flux through the sea surface between the outcrops $\sigma_1 \to \sigma$ integrated across the ocean from one coast to the other (see Fig. 2a):

$$\hat{J}_z(\sigma) = \int_{\sigma_1}^{\sigma} J_z\, dA,$$

where dA is a surface area element.

The PV flux in the infinitesimal range σ to $\sigma + d\sigma$ is $(\partial\hat{J}_z/\partial\sigma)\, d\sigma$ and can be written

$$\frac{\partial}{\partial\sigma}\left[\int_{\sigma_1}^{\sigma} J_z\, dA\right] = \int_C J_z|\nabla\sigma|^{-1}\, ds = \int_C \frac{\partial\pi}{\partial s}\, ds = \Delta\pi, \qquad (17)$$

where C is the outcrop and we have used Eq. (16) and the Leibnitz theorem (Marshall et al. 1999, p. 552). Thus a relation of diagnostic value results:

The net PV flux through the sea surface between the outcrops σ and $\sigma + d\sigma$ can be diagnosed from the difference between the Bernoulli function at the two ends of the outcrop. If π rises (falls) along an outcrop moving along it from west to east, then the net PV flux is out of (into) the ocean in the interval σ to $\sigma + d\sigma$.

2) TIME DEPENDENCE

In the time-dependent case we must retain time derivatives. Using the Leibnitz theorem and Eq. (13) we have

$$\frac{\partial}{\partial\sigma}\left[\int_{\sigma_1}^{\sigma} J_z\, dA\right] = \int_C J_z|\nabla\sigma|^{-1}\, ds = \int_C \omega_z\frac{\partial\sigma}{\partial t}|\nabla\sigma|^{-1}\, ds + \int_C \mathbf{k}\cdot\left(\frac{\partial\mathbf{u}}{\partial t}\times\nabla\sigma\right)|\nabla\sigma|^{-1}\, ds + \int_C \mathbf{k}\cdot(\nabla\pi\times\nabla\sigma)|\nabla\sigma|^{-1}\, ds.$$

To lowest order in Rossby number, and making use of (17), the above reduces to

$$\frac{\partial}{\partial\sigma}\left[\int_{\sigma_1}^{\sigma} J_z\, dA\right] = -\int_C f v_\sigma\, ds + \Delta\pi, \qquad (18)$$

where

$$v_\sigma = -|\nabla\sigma|^{-1}\frac{\partial\sigma}{\partial t}$$

is the velocity of the outcrop in the direction normal to itself, ω_z has been replaced with f, and $\Delta\pi$ is the drop in the value of the Bernoulli function from one end of the outcrop to the other.

The movement of the outcrops, v_σ, can be interpreted as the result of a PV flux. As pointed out by Csanady and Vital (1996), this flux of PV is used to create/erode the seasonal thermocline as the outcrop moves south in winter and returns to the north in the summer, as sketched schematically in Fig. 2b. In section 3b we carry out the surface integral (18) over outcrop windows in a numerical simulation, following their seasonal migration.

c. Interior PV fluxes

1) PV FLUXES IN THE STRATIFIED INTERIOR

Beneath the seasonal thermocline we assume that the flow is steady, in which case Eq. (10) reduces to

$$\mathbf{J} = \nabla\pi\times\nabla\sigma = \nabla\times(\pi\nabla\sigma) = -\nabla\times(\sigma\nabla\pi). \qquad (19)$$

Thus $\mathbf{J}$ is perpendicular to $\nabla\sigma$ (recall that the $\mathbf{J}$ vectors lie in σ surfaces) but also perpendicular to $\nabla\pi$. In fact, as sketched schematically in Fig. 3, Eq. (19) tells us that the Bernoulli function π is the streamfunction for the PV flux between σ and $\sigma + d\sigma$ because it may be written

$$|\nabla\sigma|^{-1}\mathbf{J} = \mathbf{k}^\sigma\times\nabla\pi, \qquad (20)$$

where $\mathbf{k}^\sigma = -\nabla\sigma/|\nabla\sigma|$ is a unit vector normal to σ surfaces and the horizontal gradient is operating on σ surfaces. Making use of the Montgomery potential, Eq. (9), we may write the above:

$$|\nabla\sigma|^{-1}\mathbf{J} = \mathbf{k}^\sigma\times\left[\nabla M + \nabla_\sigma\left(\frac{|\mathbf{u}|^2}{2}\right)\right], \qquad (21)$$

where all velocities are evaluated on σ surfaces. To lowest order in Rossby number, the last term in (21) can be neglected and the flux of PV in the thermocline between σ and $\sigma + d\sigma$ written as

$$\mathbf{J}^{\text{thermocline}} = \mathbf{k}^\sigma\times\nabla M = f\mathbf{u}_g + \mathbf{k}^\sigma\times\frac{\Phi}{\rho_o}\nabla_\sigma\rho', \qquad (22)$$

where $\mathbf{u}_g$ is the geostrophic velocity and f the Coriolis parameter.

Note that the $\mathbf{J}$ vector in the thermocline includes a nonadvective component due to variations in in situ density along σ surfaces caused by thermobaric effects. As we shall see in section 3, this term is not always negligible and was ignored in MN.

2) SUBDUCTION RATE

Let us now consider the flux of PV down from the surface into the interior of the ocean (see Fig. 3). In the steady state the flux of PV between two π surfaces and between two σ surfaces is invariant because of the prohibition of any PV flux across density surfaces by the impermeability theorem. In the presence of a seasonal cycle, however, the flux lines will lengthen and contract as the outcrops migrate north and south (see Fig. 2b). But integrating over the seasonal cycle, so that the storage of PV in the seasonal thermocline sums to zero, we may equate the net flux across the surface to the flux

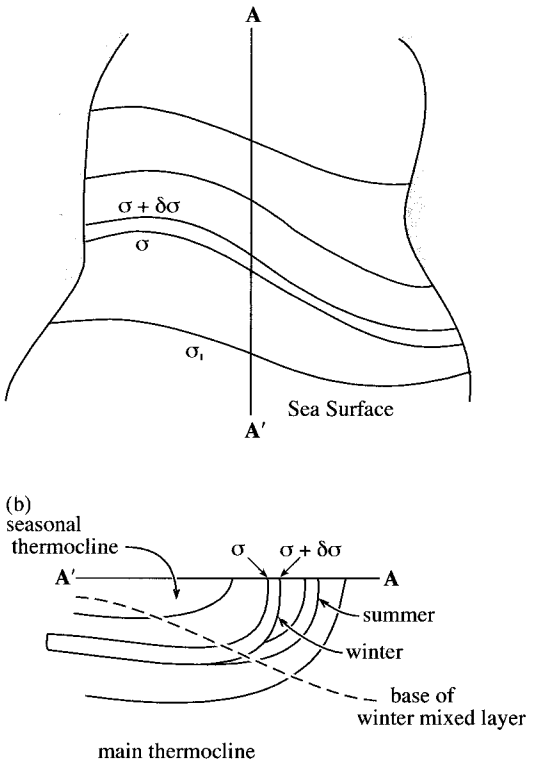

FIG. 2. (a) Schematic plan view of the outcrop window $\sigma \rightarrow \sigma + \delta\sigma$, and the reference outcrop σ_1; (b) vertical section showing the same isopycnal layer.

into the main thermocline (assuming the main thermocline is in steady state):

$$[\mathbf{J} \cdot \mathbf{n} dA]^{\text{thermocline}} = [J_z dA]^{\text{surface}},$$

where the rhs is evaluated at the sea surface (following outcrop windows), and the lhs is evaluated at a convenient level on the σ surface below the surface in the main thermocline (**n** is the unit vector normal to the top of the main thermocline and directed downward). Note how the impermeability theorem allows one to equate the flux at some distance beneath to the flux through (at) the sea surface, without reference to the (very complicated) details of the boundary-layer processes between (represented schematically in Fig. 3, by the shaded region).

If thermobaric contributions to $\mathbf{J}^{\text{thermocline}}$ can be neglected in Eq. (22), the volume of fluid entering the thermocline from the lower end of the tube directly yields the subduction rate:

$$S = -\frac{[J_z dA]^{\text{surface}}}{[\rho Q dA]^{\text{thermocline}}}, \tag{23}$$

where J_z is given by Eq. (15) integrated over the seasonal cycle. Equation (23) was written down in MN, but the derivation presented here clarifies the assumptions implicit in it and the role of the seasonal cycle.

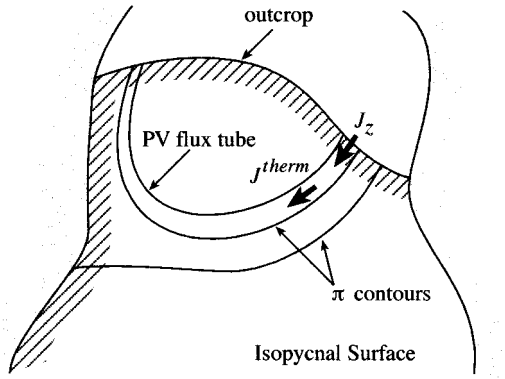

FIG. 3. The Bernoulli function π is the streamfunction for the PV flux between σ and $\sigma + \delta\sigma$, and is plotted schematically here showing subduction into the subtropical gyre.

3) PV FLUX ON A SOLID BOUNDARY

We have seen that the PV flux lines are, in fact, π contours on σ surfaces. They can close on themselves, enter and/or exit from the sea surface, but also enter and/or exit at solid boundaries (see Fig. 8 in MN). In the steady state the flux into or out of a solid boundary can be diagnosed from the variation in the Bernoulli function along the boundary [see Eq. (20)] in the σ surface that abuts it. For a detailed discussion see Csanady and Pelegri (1995) and the appendix of the present paper, in which frictional processes at the western boundary are discussed in the framework of the Stommel (1948) model.

3. Diagnosis of PV fluxes in a model of ocean circulation

To illustrate, in a less abstract way, the ideas set out in the previous section, we have diagnosed the entry, interior flux, and exit of potential vorticity into a numerical analogue of ocean circulation, using fields obtained from the North Atlantic sector of a global numerical model of ocean circulation. The model algorithm is described in Marshall et al. (1997a,b). The particular integration used here, extending from 80°S to 80°N at 1° horizontal resolution, has 20 layers in the vertical, ranging from thicknesses of 25 m at the surface to 500 m at the deepest level. Given the coarse horizontal resolution of the model baroclinic eddy transfers were parameterized. A convective adjustment scheme was used to parameterize convection. Full spherical geometry and realistic topography was employed. Density was computed using a polynomial approximation of the full equation of state. The model was initialized with the ''Levitus'' dataset and driven by 12-hourly winds and fluxes (obtained from NCEP) during the period January 1983 until January 1996.

The resulting circulation is plausible and exhibits

many realistic features and much variability both on daily, seasonal, and interannual timescales. Fields (3D velocity, pressure, temperature and salinity, air–sea fluxes) were averaged monthly and diagnostics carried out on these monthly averaged fields for the year 1992 of the simulation. The particular integration diagnosed here is discussed in more detail in Marshall et al. (1999) where the subduction and water mass transformation processes occurring in the model were diagnosed and compared with theory and models.

Before going on it is worth emphasizing that the details of the parameterization employed in the numerical model do not concern us here, inasmuch as our diagnostic relations do not make explicit reference to them. Also, we consider a PV variable with a potential density referenced to the surface. Hence, our diagnostics will be limited to the upper layers of the ocean where thermobaric effects are relatively small. Finally, the Rossby number is sufficiently small at the coarse resolution being mapped here, that $\pi \rightarrow M$ to a very good approximation [see Eqs. (8) and (9)]. In what follows π is identified with M unless noted otherwise.

a. Flux of PV through a model ocean

1) PV FLUX THROUGH THE SEA SURFACE

The annual average of J_z is evaluated from Eq. (15) summing monthly mean geostrophic velocities (calculated directly from the surface pressure field of the model) and potential densities. The annual average of the surface pressure is shown in Fig. 4a and reveals the broad sweep of the subtropical and subpolar gyres. The potential density referenced to the surface is computed from the monthly temperature and salinity using the full equation of state employed in the model. The annual average shows a broad range of σ values, from 20 at the equator off Africa to 27.4 in the Norwegian Sea (Fig. 4b). The field of J_z (Fig. 4c) shows coherent large-scale patterns; its sign depends on the orientation of $\mathbf{u}_g$ relative to $\nabla\sigma$. In the subtropical gyre, J_z is, in the main, negative and the PV flux is downward (into the ocean). Along the western boundary and at high latitudes, however, the PV flux is positive. In addition to this general pattern, we note regions of upward PV flux near the equator and over an area centered at 30°N extending from 40° to 20°W. Note, however, that the J_z field as estimated from Eq. (15) is not very meaningful near the equator where geostrophic velocities are not defined. Equation (14) should be used there. In the Labrador Sea and near the northern boundary of the domain, the PV flux is into the ocean.

2) INTERIOR FLUX—PV FLUX LINES

Equation (20) tells us that π is the streamfunction for the **J** vectors on σ surfaces. We plot π on isopycnal surfaces and relate the resulting interior flux lines to the PV flux at the surface J_z. In the interior and to lowest order in Rossby number, **J** is made up of the advective component and the nonadvective thermobaric component [see Eq. (22)]. Figures 5a and 6a show the isolines of π on isopycnals, along with the sign of J_z at the sea surface north of the outcrop (see legend). Note that the sign of J_z is in accord with the sense of the PV flux lines on the isopycnal surface: when the PV flux is downward (upward), the PV flux lines are directed away from (toward) the base of the mixed layer. This is to be expected theoretically from the impermeability theorem, and it is pleasing that this is seen diagnostically.

On the 25.4 σ surface (Fig. 5a), the PV flux at the surface is downward just north of the outcrop except in a narrow band near the western boundary where it is directed strongly outward. Over most of the gyre, the 25.4 surface is almost entirely ventilated: PV flows down from the mixed layer and then flows back into the mixed layer at the western boundary. The thermobaric contribution to the PV transport is essentially negligible on this surface (Fig. 5d) and PV is carried into the interior by geostrophic currents.

Farther north, on the 26.6 surface (Fig. 6a), PV flows down from the mixed layer between 40° and 20°W near 40°N and is carried away into the interior. Note that some flux lines close on themselves on this isopycnal surface and that others also emanate from the coast in the region of the western boundary current. At these depths, the nonadvective thermobaric flux is no longer negligible (compare Fig. 6d with Fig. 6c) and shows that the Bernoulli function is not a streamfunction for the geostrophic flow on isopycnals. This has been pointed out, for example, by McDougall (1989) and Zhang and Hogg (1992), but is seen here through the **J**-vector framework. It should be remembered, however, that the Bernoulli function is always an exact streamfunction for the total PV flux in the steady state.

3) SUBDUCTION RATES FROM **J** VECTORS

The annual subduction rate is computed from Eq. (23), making use of the J_z plotted in Fig. 4c. We compute S across the surface defined by the depth, H, of the potential vorticity maximum $Q_{\max}$ in March 1992 plotted in Fig. 7a. This ensures that the computation is stable and robust and avoids dividing by a vanishingly small, ill-defined stratification at the base of the mixed layer. The resulting H is generally slightly deeper than the mixed layer depth diagnosed by standard procedures and is perhaps best thought of as representing the top of the main thermocline. Nevertheless, it shows the same broad structure with a familiar tongue of somewhat deeper—200 m thick—layers extending southwestward across the basin; H is particularly deep in the Labrador Sea where it exceeds 2 km. In fact, the winter of 1991/92 was characterized by huge buoyancy losses over the

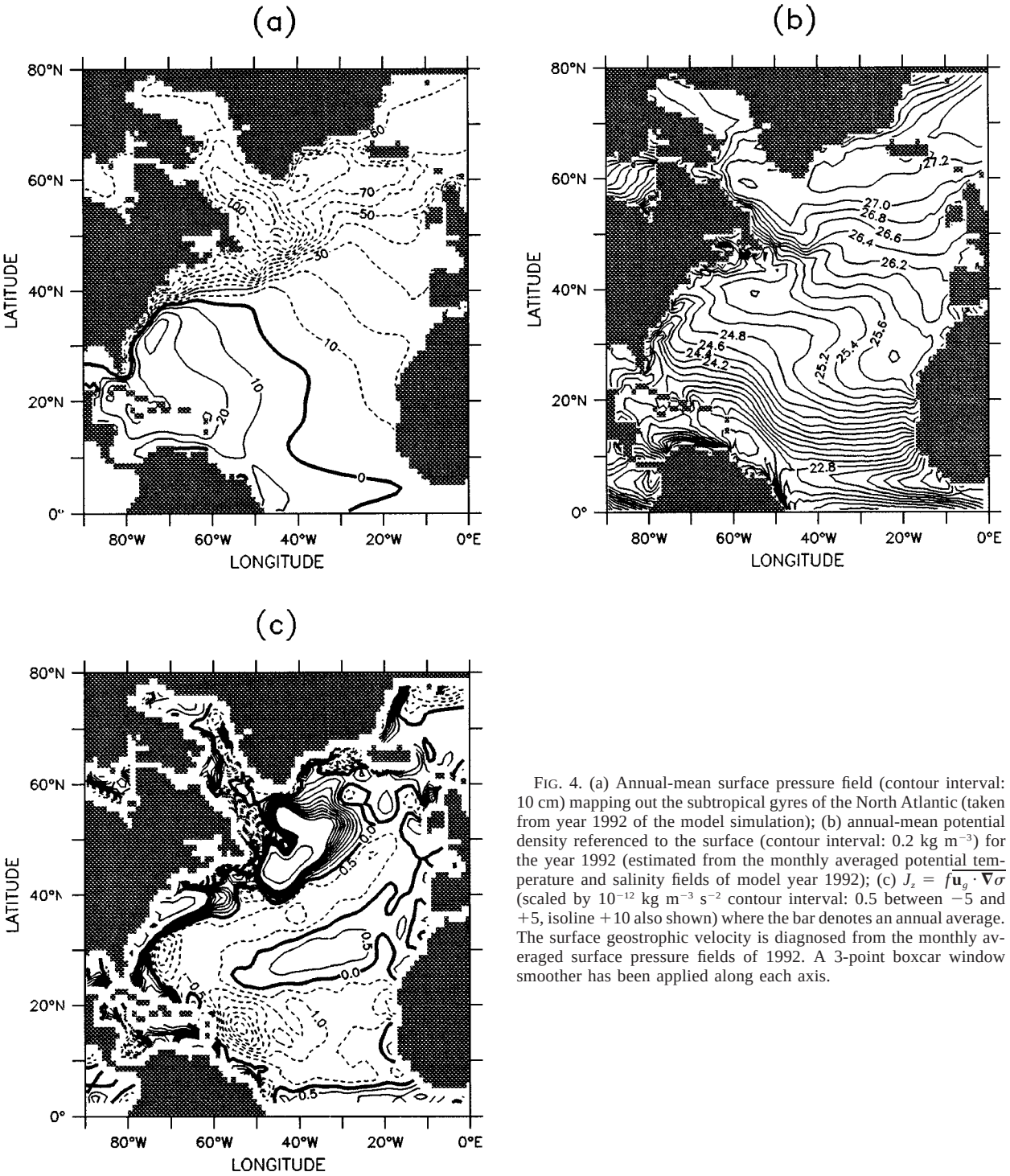

FIG. 4. (a) Annual-mean surface pressure field (contour interval: 10 cm) mapping out the subtropical gyres of the North Atlantic (taken from year 1992 of the model simulation); (b) annual-mean potential density referenced to the surface (contour interval: 0.2 kg m^{-3}) for the year 1992 (estimated from the monthly averaged potential temperature and salinity fields of model year 1992); (c) $J_z = f\overline{\mathbf{u}_g \cdot \nabla\sigma}$ (scaled by 10^{-12} kg m^{-3} s^{-2} contour interval: 0.5 between -5 and $+5$, isoline $+10$ also shown) where the bar denotes an annual average. The surface geostrophic velocity is diagnosed from the monthly averaged surface pressure fields of 1992. A 3-point boxcar window smoother has been applied along each axis.

Labrador Sea and deep water was found at a depth of 2500 m.

The resulting subduction rate, along with an estimate made using the kinematic definition—the method is described in Marshall et al. (1993)—are shown in Figs.7b and 7c, respectively. The agreement between the two estimates is encouraging: there is a broad area of subduction over the subtropical gyre with a narrow zone of values between 100 and 250 m yr^{-1} extending from 30°N, 70°W to 50°N, 20°W. Another area of smaller

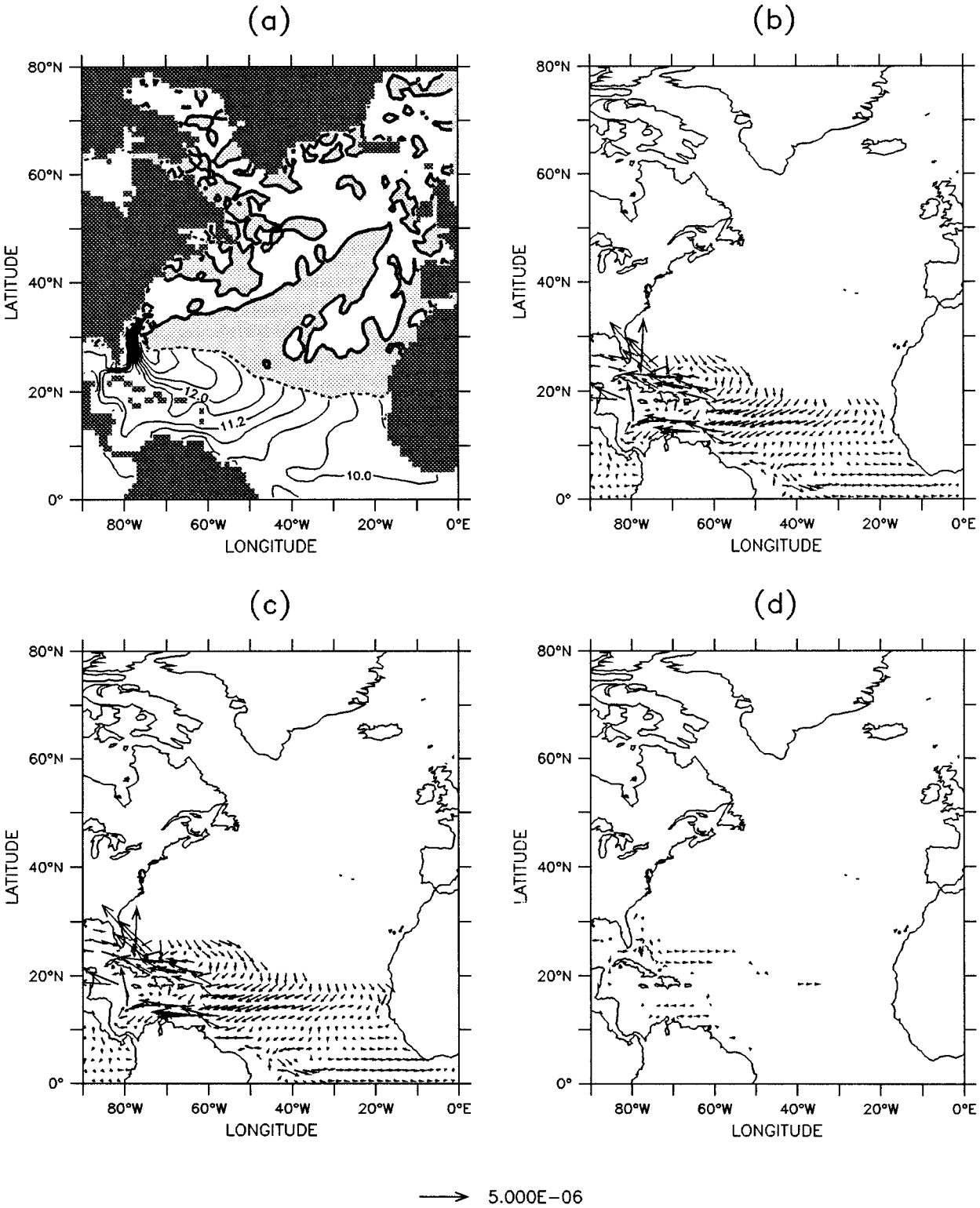

FIG. 5. The Bernoulli function, π, and the PV flux **J** on isopycnal surface 25.4 for March 1992: (a) π (contour interval: 0.4 m^2 s^{-2}) and J_z. The dotted line denotes the outcrop. The thin solid lines show the π isolines south of the outcrop, and the thick solid lines show the zero J_z contour north of the outcrop. Regions where J_z is negative have been shaded in gray. (b) The PV flux **J** at lowest order in Rossby number as given by Eq. (22). The scaling is given by an arrow of magnitude 5×10^{-6} m s^{-2} (corresponding to a speed of 5 cm s^{-1} if $f = 10^{-4}$ s^{-1}). (c) Advective component $f\mathbf{u}_g$ (d) nonadvective thermobaric component $\mathbf{k}^\sigma \times \rho_o^{-1}\mathbf{\Phi}\nabla_\sigma\rho'$. Note that to allow visualization of the vectors the land has not been shaded in (b), (c), and (d) and vectors greater than $5\sqrt{2} \times 10^{-6}$ m s^{-2} have not been plotted.

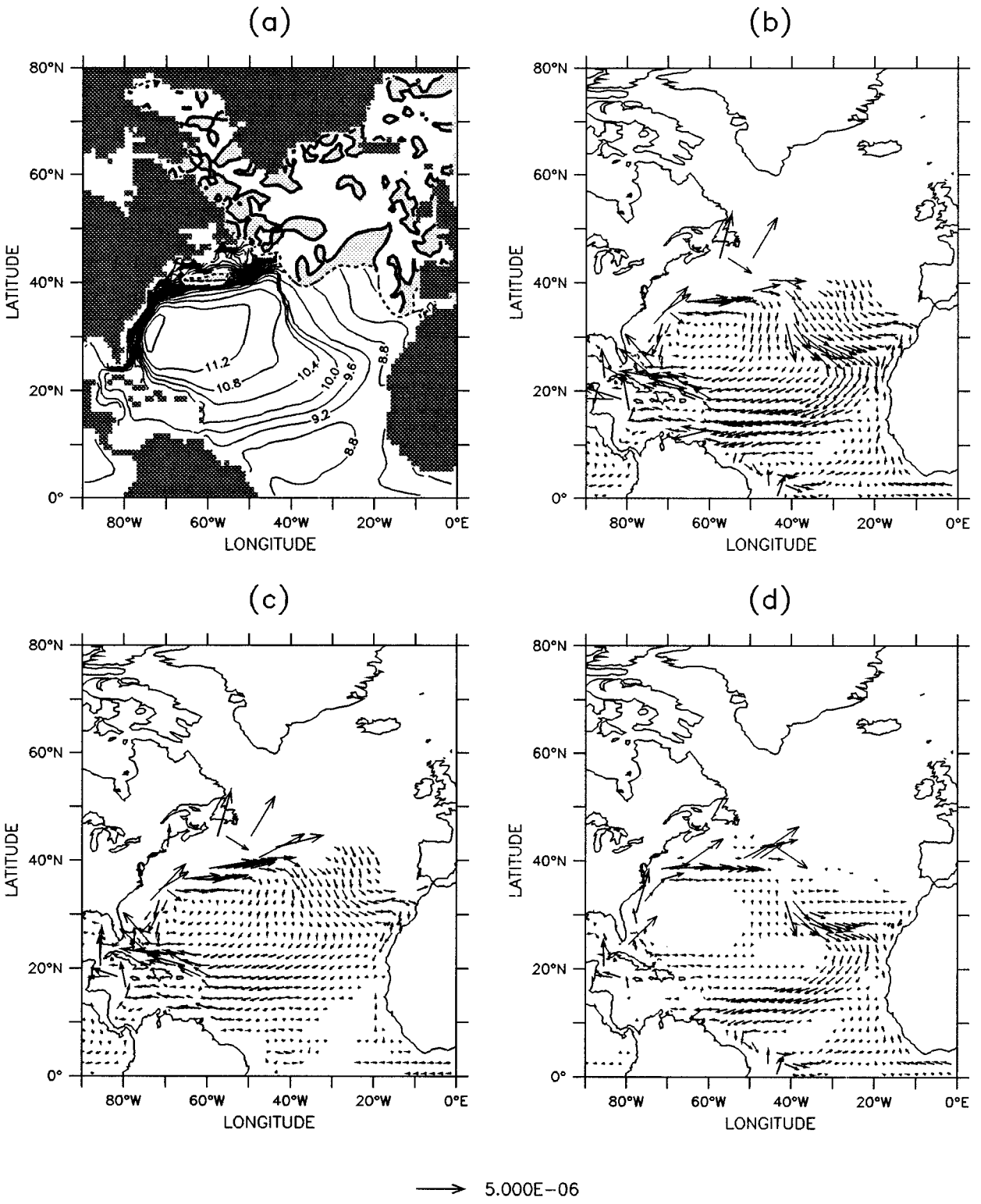

FIG. 6. Same as Fig. 5 but on isopycnal surface 26.6.

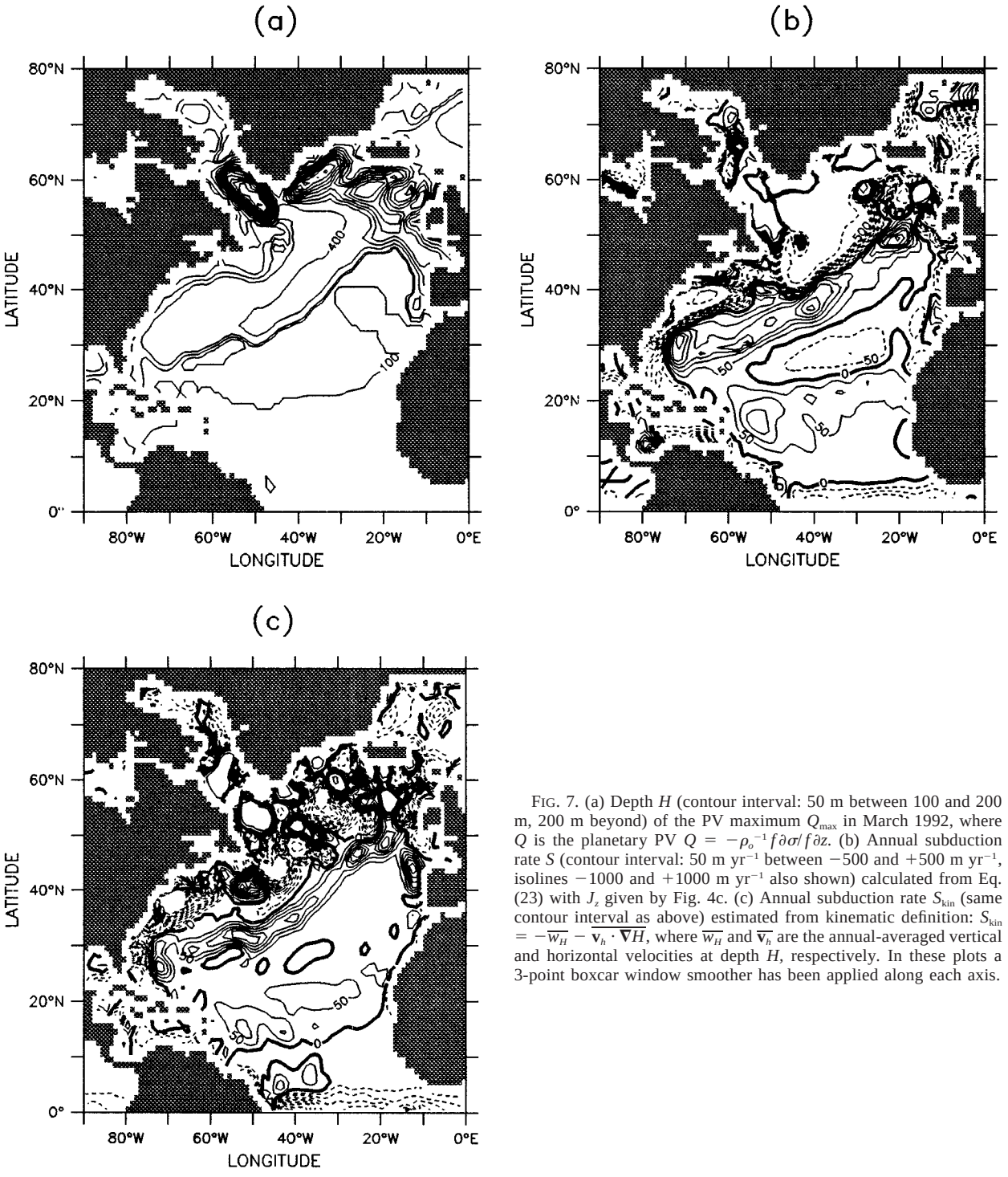

FIG. 7. (a) Depth H (contour interval: 50 m between 100 and 200 m, 200 m beyond) of the PV maximum $Q_{\max}$ in March 1992, where Q is the planetary PV $Q = -\rho_o^{-1} f \partial\sigma/f\partial z$. (b) Annual subduction rate S (contour interval: 50 m yr^{-1} between -500 and $+500$ m yr^{-1}, isolines -1000 and $+1000$ m yr^{-1} also shown) calculated from Eq. (23) with J_z given by Fig. 4c. (c) Annual subduction rate S_{kin} (same contour interval as above) estimated from kinematic definition: $S_{\text{kin}} = -\overline{w_H} - \overline{\mathbf{v}_h \cdot \nabla H}$, where $\overline{w_H}$ and $\overline{\mathbf{v}_h}$ are the annual-averaged vertical and horizontal velocities at depth H, respectively. In these plots a 3-point boxcar window smoother has been applied along each axis.

values (50–100 m yr^{-1}) is found across the basin between roughly 10° and 20°N. In the vicinity of the equator, along the western boundary, and at high latitudes, the two estimates show generally large entrainment rates.

b. Integral fluxes

We now diagnose the quantities $\partial\hat{J}_z(\sigma)/\partial\sigma$ and $\int_C d\pi$ described in section 2b(2) [see Eq. (17)]. The former is evaluated by adding the contributions (Fig. 4c) $J_z dA$ for

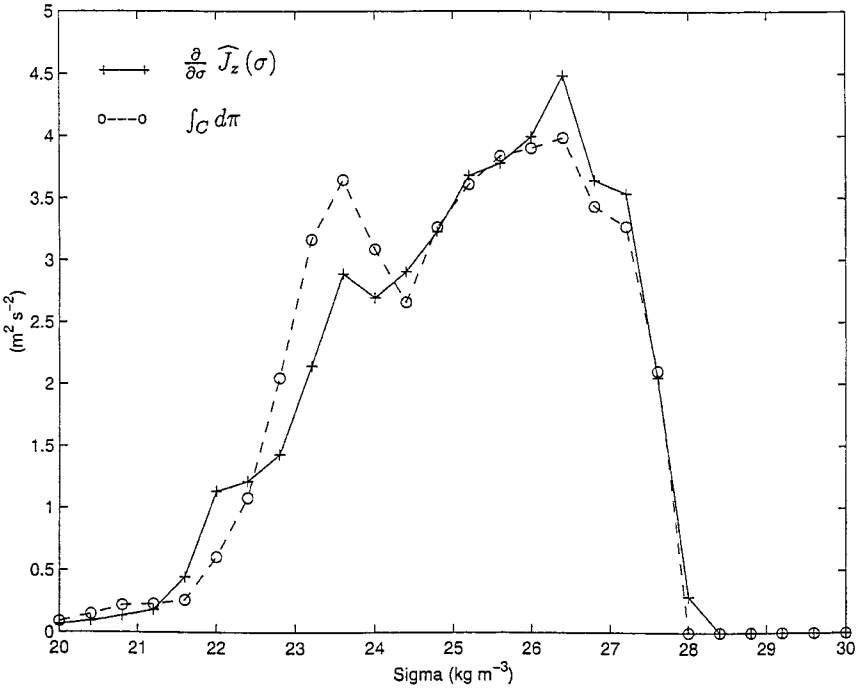

FIG. 8. Annual average of $\partial\hat{J}_z(\sigma)/\partial\sigma$ as a function of σ (solid line) and annual average of $\int_C d\pi$ as a function of σ (dotted line).

grid points whose densities lie between $\sigma - \delta\sigma/2$ and $\sigma + \delta\sigma/2$, where the density bin, $\delta\sigma$, is set to 0.4. This is done over outcrop windows each month, following their seasonal migration, and then summing to form the annual average. The annual average over 1992 is shown in Fig. 8; $\partial\hat{J}_z(\sigma)/\partial\sigma$ is positive for all density ranges with a maximum of 4.5 $m^2\ s^{-2}$ at $\sigma = 26.4$. We see that, even though there is a widespread area of negative J_z in the subtropical gyre (see Fig. 4c), the intense positive fluxes localized on the western boundary dominate the integral. As a check on our calculation we evaluate the rhs of (17) by summing $d\pi$ along the faces separating grid cells with densities greater than σ from grid cells with densities lees than σ. The annual average displays essentially the same structure as $\partial\hat{J}_z(\sigma)/\partial\sigma$. For the most part, the residuals are less than 0.5 $m^2\ s^{-2}$ and are due to numerical differences in the way the two quantities are evaluated.

We see, then, that the annually averaged flux of PV, integrated over each density class, is directed *from* the ocean *to* the atmosphere. This might be expected since the net flux depends only on the difference in the Bernoulli function at the two ends of the outcrop [see Eq. (17)] and hence, to a good approximation, to the difference in pressure at the sea surface at the coasts (the term $\rho' gz$ remaining constant along the outcrop). Outcrops attach to the boundary on the west where, due to the southeast to northwest tilt of the outcrops, it is denser (colder) there. Hence the pressure at the sea surface is typically lower in the west than in the east: $\pi_{\text{east}} > \pi_{\text{west}}$ implying that $\hat{J}_z(\sigma)$ is positive. This is achieved by a flux of PV from the western boundary [as in (4) of the schematic diagram of MN, Fig. 8], revealing a fascinating connection between mechanical and thermodynamic processes exposed by the **J**-vector framework.

4. Discussion

We have extended the PV theory presented in MN—through the lens of the generalized Bernoulli theorem derived by Schär (1993) in the atmospheric context—and have derived and interpreted very general, yet very simple, expressions that quantify the flux of PV across the sea surface and its transport through and exit from the ocean. Illustration of these expressions through diagnosis of a general circulation model has allowed us to look at PV flux patterns in a more realistic context than the idealized examples of MN.

Ocean ventilation and recirculation can be understood from a PV flux budget perspective. PV flows into (out of) the ocean wherever, following the geostrophic flow, potential density at the sea surface increases (decreases). In the subtropical gyre, PV flows down from the surface into the interior, circulates on isopycnal surfaces, and exits at the sea surface on the western margin of the gyre. Figures 5a and 6a have several features in common with the isopycnal maps of planetary PV calculated from gridded hydrographic data by McDowell et al. (1982). If the thermocline is steady, adiabatic, and inviscid, the PV contours and the streamlines coincide on an isopycnal surface. Thus Figs. 5a and 6a ought to delineate the gross features of the PV distribution away from the

boundaries. The use of low-resolution data and planetary PV cause the PV contours of McDowell et al. to approach the boundary in a zonal manner. In our computation, however, many of the **J**-vector flux tubes (or the Bernoulli contours) are deflected toward the northeast before they hit the coast. Our maps suggest that many of the PV contours on shallow σ surfaces wrap themselves around the central subtropical gyre and return to the outcrop to the west.

Integrated across the outcrop, we have derived a simple diagnostic relation between the net flux of PV and the difference in Bernoulli function from one end of the outcrop to the other. There is a net flux of PV out of isopycnal layers, across the sea surface, if $\pi_{\text{east}} > \pi_{\text{west}}$. In the model studied here, and we suspect in the real Atlantic Ocean too, when integrated over an outcrop window we always find a net PV flux out of the ocean because the pressure at the sea surface is always higher at the eastern margin of an outcrop than at its western margin. This excess flux must emanate from the western boundary layer [flux line (4) in MN's Fig. 8]. There is a basin-integrated near-surface geostrophic mass transport directed poleward, up the density gradient. As Eq. (15) shows, the Ekman transport does not enter into the diagnosis of the surface PV flux. Calculations of the diapycnal volume flux (made on the same model output: Marshall et al. 1999, their Fig. 7) shows that the basin-integrated flow in the upper layer is indeed directed poleward except at the very lowest densities ($\sigma < 23$).

From the impermeability theorem, the (nonadvective) flux of PV through the sea surface must be associated with an advective (subducted) flux between the upper ocean and the main thermocline, provided thermobaric effects are negligible. Patterns of subduction rates using the PV flux framework are very similar to those computed directly.

It is perhaps surprising that expressions of such generality are at the same time so succinct, that they do not make explicit reference to PV frictional and buoyancy forcing terms, and that they are rather readily and robustly computed from models (or observations). The simplicity is, however, perhaps illusory [see the cautionary note in Rhines (1993)]; the flux form of the potential vorticity equation distracts us away from many important details. For example, although Eq. (13) is completely general and can be computed from knowledge of π and σ alone, the patterns of π and σ owe their existence to PV forcing terms. Nevertheless, **J** vectors provide an interesting and elegant perspective on the fluid mechanics of ocean circulation.

Acknowledgments. John Marshall and Daniel Jamous would like to thank the Physical Oceanography section of NSF for their support, which made this work possible. The comments of two perceptive and patient reviewers are gratefully acknowledged.

APPENDIX

The Flux Form of the PV Equation for the Stommel's Gyre

In the archetypal study of Stommel (1948) of a wind-driven gyre in a homogeneous ocean, the PV variable is simply the vertical component of the absolute vorticity $q = \mathbf{k} \cdot \boldsymbol{\omega}$, where $\mathbf{k}$ is the unit vertical vector and $\boldsymbol{\omega}$ the absolute vorticity given by (3). From the definition (3) we may write

$$\frac{\partial q}{\partial t} + \boldsymbol{\nabla} \cdot \mathbf{j} = 0, \tag{A1}$$

where

$$\mathbf{j} = \mathbf{k} \times \frac{\partial \mathbf{u}}{\partial t}$$

is defined up to a nondivergent vector. But from the momentum equation:

$$\frac{\partial \mathbf{u}}{\partial t} + (\mathbf{k} \times \mathbf{u})q + \boldsymbol{\nabla}\pi = \mathbf{F}, \tag{A2}$$

where π is the Bernoulli function, we may write

$$\mathbf{k} \times \frac{\partial \mathbf{u}}{\partial t} - \mathbf{u}q + \mathbf{k} \times \boldsymbol{\nabla}\pi = \mathbf{k} \times \mathbf{F}, \tag{A3}$$

which can be expressed as

$$\mathbf{J} = \mathbf{k} \times \left(\frac{\partial \mathbf{u}}{\partial t} + \boldsymbol{\nabla}\pi \right), \tag{A4}$$

where

$$\mathbf{J} = q\mathbf{u} + \mathbf{k} \times \mathbf{F}. \tag{A5}$$

Equation (A3) is the analog of (7), Eq. (A4) the analog of (10), and (A5) the analog of (11).

We note in passing that the momentum equation, written in terms of **J**, takes the compact form

$$\frac{\partial \mathbf{u}}{\partial t} + \mathbf{k} \times \mathbf{J} = -\boldsymbol{\nabla}\pi, \tag{A6}$$

which looks very similar to the isentropic coordinate version of the momentum equation of a stratified fluid [see Eq. (26) of Schär (1993)].

The analysis presented in this study is based on Eq. (A4) and it enables us to plot **J,** in the steady state at least, from knowledge of the Bernoulli function, π, alone. Figure A1 plots **J** for the Stommel gyre from the Bernoulli function, which in Stommel's case reduces to the surface pressure field. It displays **J** directed outward from the western boundary (where frictional contributions to **F** are important), southward, and then back in to the boundary to the south. Hence the interest in Eq. (A4), which does not make explicit reference to **F** (and buoyancy forcing in the more general case). In this paper the above framework has been generalized to capture exit and entry of PV in a stratified ocean not just from

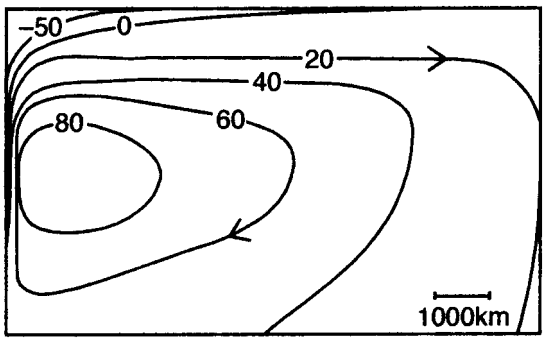

FIG. A1. Surface height contours (cm) for the Stommel subtropical gyre [after Fig. 6 of Stommel (1948)]. The arrows show the sense of the **J** vectors.

the solid boundaries but also from the sea surface via the outcrops.

REFERENCES

Bretherton, C. S., and C. Schär, 1993: Flux of potential vorticity substance: A simple derivation and a uniqueness property. *J. Atmos Sci.,* **50,** 1834–1836.

Csanady, G. T., and J. L. Pelegri, 1995: Vorticity balance of boundary currents. *J. Mar. Res.,* **53,** 171–187.

——, and G. Vittal, 1996: Vorticity balance of outcropping isopycnals. *J. Phys. Oceanogr.,* **26,** 1952–1956.

Haynes, P. H., and M. E. McIntyre, 1987: On the evolution of vorticity and potential vorticity in the presence of diabatic heating and frictional or other forces. *J. Atmos. Sci.,* **44,** 828–841.

Marshall, J. C., and A. J. G. Nurser, 1992: Fluid dynamics of thermocline ventilation. *J. Phys. Oceanogr.,* **22,** 583–595.

——, ——, and R. G. Williams, 1993: Inferring the subduction rate and period over the North Atlantic. *J. Phys. Oceanogr.,* **23,** 1315–1329.

——, C. Hill, L. Perelman, and A. Adcroft, 1997a: Hydrostatic, quasi-hydrostatic, and nonhydrostatic ocean modeling. *J. Geophys. Res.,* **102** (C3), 5733–5752.

——, A. Adcroft, C. Hill, L. Perelman, and C. Heisey, 1997b: A finite-volume, incompressible Navier Stokes model for studies of the ocean on parallel computers. *J. Geophys. Res.,* **102** (C3), 5753–5766.

——, D. Jamous, and J. Nilsson, 1999: Reconciling ''thermodynamic'' and ''dynamic'' methods of computation of water-mass transformation rates. *Deep-Sea Res.,* **46,** 545–572.

McDougall, T. J., 1988: Neutral surface potential vorticity. *Progress in Oceanography,* Vol. 20, Pergamon, 185–221.

——, 1989: Streamfunctions for the lateral velocity vector in a compressible ocean. *J. Mar. Res.,* **47,** 267–284.

McDowell, S., P. Rhines, and T. Keffer, 1982: North Atlantic potential vorticity and its relation to the general circulation. *J. Phys. Oceanogr.,* **12,** 1417–1463.

Rhines, P. R., 1993: Oceanic general circulation: Wave and advection dynamics. *Modeling Oceanic Climate Interactions,* J. Willebrand and D. L. T. Anderson, Eds., NATO ASI Series, Vol. III, Springer-Verlag.

Schär, C., 1993: A generalization of Bernoulli's theorem. *J. Atmos. Sci.,* **50,** 1437–1443.

Stommel, H., 1948: The westward intensification of wind-driven currents. *Trans. Amer. Geophys. Union,* **29,** 202–206.

Zhang, H. M., and N. G. Hogg, 1992: Circulation and water mass balance in the Brazil Basin. *J. Mar. Res.,* **50,** 385–420.